PAPER

Check for updates

Synthesis of bimetal MOFs for rapid removal of doxorubicin in water by advanced oxidation method†

Junhao Hu, [ID] ‡[a] Qiong Yi,‡[a] Ziyi Xiao,[a] Feng Tian, [ID] [a] Tingting Shu,[a] Xiaolan Liu,[a] Yingxi Wang,[a] Ling Li [ID] *[a] and Jiangang Zhou*[b]

Doxorubicin (DOX) has been an emerging environmental pollutant due to its significant genotoxicity to mankind. Advanced oxidation processes are a potential strategy to remove DOX in water solution. To develop a highly efficient catalytic agent to remove DOX, bimetal MOFs were synthesized, with Cu^{2+} and Co^{2+} as the central ions and adenine as the organic ligand. This study investigated the degradation of DOX by Co/Cu-MOFs combined with peroxymonosulfate (PMS). It was found that the degradation of DOX by Co/Cu-MOFs can reach 80% in only 10 seconds. This can be explained by the charge transfer from Co(III) to Co(II) being accelerated by Cu^{2+}, resulting in the rapid generation of free radicals, which was proved by the EIS Nyquist diagram. Co/Cu-MOFs can be reused by simply washing with water without inactivation. Therefore, Co/Cu-MOFs can be used as an efficient catalytic agent to degrade DOX in environmental water.

1. Introduction

In the last few decades, pharmaceutical and personal care products (PPCPs) have been developed and used in large quantities.[1] Among them, doxorubicin hydrochloride (DOX) is the most common anti-cancer drug that has frequently been reported to have been detected in sewage systems.[2,3] With the widespread use of DOX in tumor treatment, DOX enters groundwater and penetrates into the soil, causing DOX to accumulate easily in plants and eventually to enter the human body through the food chain.[4] Unfortunately, when DOX is accumulated to a certain extent, it will cause the body's immune system to decline and cause pollution to the natural environment.[5] The contamination of a water body with DOX residues represents a growing environmental problem, so the removal of DOX from contaminated water is very meaningful.

In the past few years, various classic methods and technologies have been studied in the elimination of pharmaceuticals from water, such as functionalized mesoporous silicas,[6] iron oxide nanoparticles,[7] and magnetic particles.[8] However, these methods only physically separate pharmaceuticals from water and cannot efficiently remove contaminants from water due to

some limitations, such as secondary pollution, high cost and difficult-to-remove organic contaminants. Hence, it is of great significance to develop efficient and low-cost methods to eliminate antibiotics in the aquatic environment.

In recent years, advanced oxidation processes (AOPs) have been considered one of the most effective methods to destroy difficult-to-degrade organic pollutants by highly oxidizing free radicals without producing secondary pollution.[9,10] Commonly used oxidants include peroxymonosulfate (PMS), peroxodisulfate (PDS), and hydrogen peroxide (H_2O_2). PMS is usually more easily activated than PDS due to its asymmetric structure.[11] More notably, compared with hydroxyl radicals ($\cdot OH$) obtained by catalyzing H_2O_2, sulfate radicals ($SO_4^{-\cdot}$) obtained by catalyzing PMS show remarkable advantages, such as high oxidizing ability, long lifetime of active radicals, high selectivity and efficiency with organic compounds over a wide pH range, and they are gaining more interest.[12–15] However, ($SO_4^{-\cdot}$)-based AOPs still have certain limitations in that insufficient catalyst activity of the catalytic agents results in the incomplete degradation of pharmaceuticals. Improving the catalytic activity of a catalyst has become a hotspot in research into the degradation of pharmaceuticals.[16,17] To date, few studies have investigated the removal of DOX by AOPs.[18–20] Therefore, it is meaningful to design a highly efficient catalytic agent to activate persulfate to generate enough $SO_4^{-\cdot}$ to remove DOX.

Metal organic framework (MOF) materials are a kind of functional material with a three-dimensional network structure formed by coordination of metal ions and organic ligands.[21] With an ideal topological structure, high porosity, adjustable pore size and large specific surface area, MOFs have aroused

[a]Ministry-of-Education Key Laboratory for the Synthesis and Application of Organic Function Molecules, Hubei University, 430062, China. E-mail: lingli@hubu.edu.cn
[b]Faculty of Resources and Environmental Science, Hubei University, 430062, China. E-mail: 497966492@qq.com

‡ These authors contributed equally to this work.

great interest among researchers.[22–25] Cao *et al.* added Co to UiO-66 for the efficient catalytic removal of TC and the porosity of UiO-66 provided active sites for contact between the catalyst and TC molecules.[26] The removal and catalytic degradation of persistent organic pollutants in water based on MOFs is a promising water treatment technology, but its application is limited due to its poor thermal, chemical and hydrolytic stability.[27] In recent years, since aromatic N heterocyclic compounds have been found with good catalytic activity and stability, aromatic N heterocyclic ligands have been used to construct MOFs. Adenine contains a large number of nitrogen atoms in coordination with metal ions, which can enhance the stability of the material, and also contains an amino group, which serves as a Lewis basic site to effectively adsorb DOX molecules, potentially improving the degradation effect.[28–30]

Because Co^{2+} can activate peroxymonosulfate very well to produce sulfate radicals ($SO_4^{-·}$) for the degradation of organic pollutants,[31,32] a large number of cobalt-based MOFs have been reported for use in the field of catalytic degradation.[33–35] However, most single-metal MOFs are unstable in aqueous solution. Compared with single-metal MOFs, bimetal MOFs have more adjustable active sites, and the synergistic effect between bimetals can achieve better catalytic activity. Inspired by this, we selected Co^{2+} and Cu^{2+} as the central metal ions and used adenine as the organic ligand to construct Co/Cu-MOFs, which were used to remove residual anticancer drug doxorubicin hydrochloride (DOX) from water. To the best of the authors' knowledge, this study is among the first to investigate the degradation of DOX by bimetal MOFs combined with PMS.

2. Experimental

2.1 Materials and instruments

Copper acetate monohydrate ($C_4H_6CuO_4·H_2O$), cobalt(III) acetate tetrahydrate ($C_4H_6CoO_4·4H_2O$), potassium monopersulfate triple salt (42–46% $KHSO_5$ basis), and adenine were purchased from Shanghai Macklin Biochemical Co., Ltd. Doxorubicin (DOX) and absolute ethanol were purchased from Aladdin Chemistry, Co. (Shanghai) and used as received. *N,N*-dimethylformamide (C_3H_7NO, DMF) was purchased from Sinopharm Chemical Reagent Co., Ltd. Aqueous solutions were prepared with deionized water. All other chemicals used in this work were of analytical grade, obtained from commercial suppliers, and used without further purification unless otherwise noted.

The powder X-ray diffractometry (XRD) patterns were obtained using a D8 advance X-ray diffractometer (Bruker Company, Germany). Fourier transform infra-red (FT-IR) spectra were obtained using a spectrum one FT-IR spectrophotometer (PerkinElmer, USA) at room temperature. Morphologies of the samples were observed on a JSM6510LV scanning electron microscope (SEM, JEOL, Japan). The elemental composition of the sample was analyzed using energy dispersive X-ray spectroscopy (EDX) and elemental mapping in a Super-XTM system.

2.2 Synthesis of materials

Co/Cu-MOFs were synthesized by a hydrothermal method. Typically, 0.0498 g of $C_4H_6CoO_4·4H_2O$ and 0.04993 g of $C_4H_6CuO_4·H_2O$ were sonicated in 8 mL of DMF. At the same time, 0.1622 g of adenine was sonicated in 24 mL of DMF until completely dissolved. Then, the two solutions were mixed and transferred to a polytetrafluoroethylene reactor, and 0.1 mL of water was added. After that, the polytetrafluoroethylene reactor was put into a program-controlled oven. The temperature was raised to 120 °C at a heating rate of 1 °C min^{-1}, and the reaction lasted for 24 h. After centrifugal separation, the obtained product was washed three times with 54 mL of DMF to get rid of unreacted compositions, and dried overnight at 130 °C to obtain Co/Cu-MOFs, which were stored for later use. Different conditions for the controlled synthesis of Co/Cu-MOFs are shown in Table S1.†

2.3 Catalytic degradation of DOX

Briefly, 5 mg of Co/Cu-MOFs was first added to 100 mL of DOX solution (20 mg L^{-1}) and stirred for 30 minutes to reach adsorption–desorption equilibrium. Then, 5 mg of PMS was weighed and added immediately to the reaction solution to initiate the oxidation process. The temperature of the reaction was maintained at 25 °C and the solution was mechanically stirred at 400 rpm. At regular intervals (0–5 min), water samples were taken and filtered with a 45 mm PTFE syringe filter, and then 0.5 mL of methanol was added as a quencher to stop further reaction. The absorbance of the filtered water sample was measured at a wavelength of 480 nm on an ultraviolet spectrophotometer, and the concentration of DOX was calculated according to the standard curve to obtain the adsorption rate and the degradation rate. After each degradation experiment, the used Co/Cu-MOFs were washed with DMF and dried overnight at 130 °C for the recycling experiment. All experiments were repeated three times to ensure the accuracy of the experimental results.

In order to determine the concentration of DOX accurately, as shown in Fig. S1,† the working curves of doxorubicin in different concentration ranges were measured. When the concentration of DOX was in the range of 0.001–0.01 g L^{-1}, the concentration was determined according to the equation $A = 21.63518C + 0.0008782$; when the concentration of DOX was in the range of 0.01–0.1 g L^{-1}, the concentration was determined according to the equation $A = 16.45999C + 0.11248$. In both equations, C is the concentration of DOX and A is the absorbance of the solution.

3. Results and discussion

3.1 Characterization results

The XRD patterns of Co-MOFs, Cu-MOFs and Co/Cu-MOFs-1–7 are shown in Fig. 1 (the synthesis conditions of the Co/Cu-MOFs-1–7 are shown in Table S1†). The XRD patterns are consistent with previous studies on successfully synthesized Co-MOFs and Cu-MOFs.[36,37] The XRD diffraction peaks of Co/Cu-MOFs were different from those of Co-MOFs and Cu-MOFs,
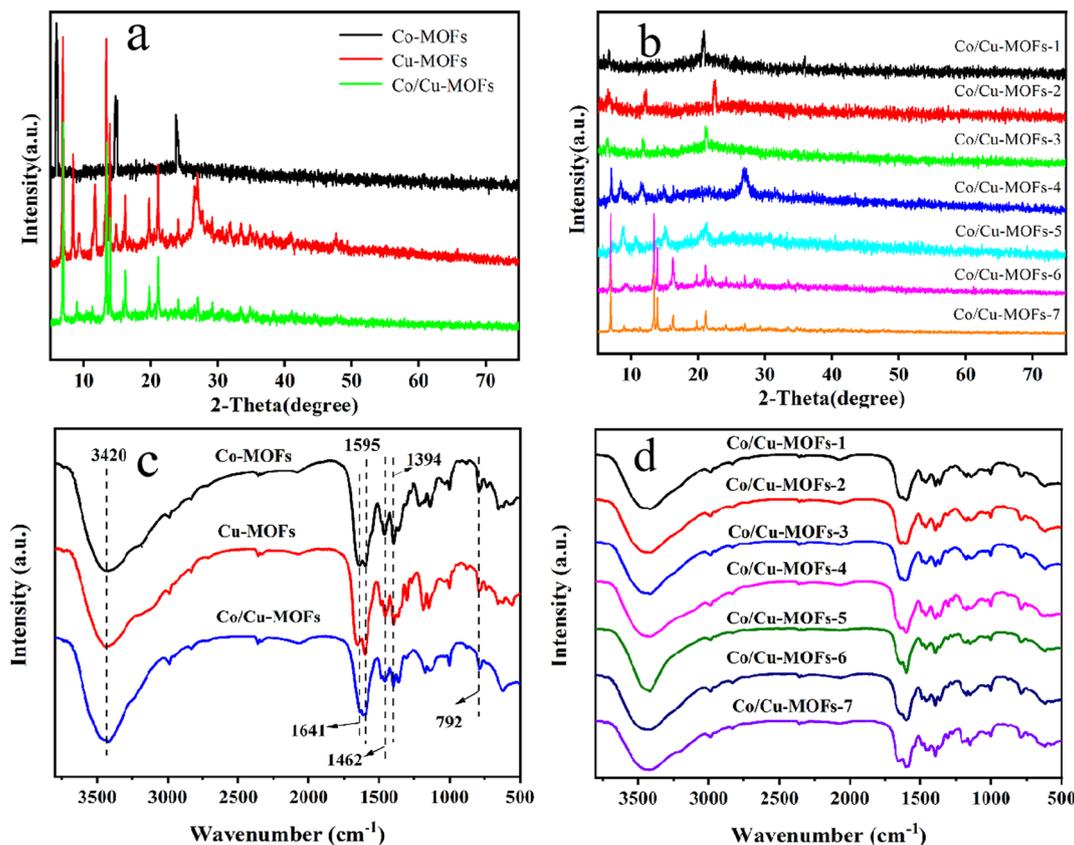
Fig. 1 (a and b) XRD patterns, (c and d) FT-IR spectra of different MOFs.

indicating that Co/Cu-MOFs are not a simple mixture of Co-MOFs and Cu-MOFs, but a new type of MOF. It can also be seen from Fig. 1b that as the ratio of Co^{2+}/Cu^{2+} varies, the XRD diffraction peaks are different from each other, indicating that the structure of Co/Cu-MOFs can be controlled by adjusting the ratio of different metal ions.

FT-IR spectra were collected using powder samples from 500 to 4000 cm^{-1} to confirm linkage of metal ions and adenine and the presence of functional groups in the MOFs, as shown in Fig. 1c and d. The bands in the range of 800–500 cm^{-1} are attributed to the stretching vibration of Co nodes.[38,39] The bands on show in 1500–1600 cm^{-1} are the stretching and bending modes of the imidazole ring of adenine and, in particular, the strong peak at 1595 cm^{-1} shows the presence of C–N bending.[38] A series of characteristic absorption peaks appeared in the range of 1300–1450 cm^{-1}, especially at 1394 cm^{-1}, which represent the vibrations of C–H in adenine.[40] The broad band centered at 3420 cm^{-1} originated from the O–H stretching vibration of water molecules adsorbed on the catalyst surface.

A series of Co/Cu-MOFs (Co/Cu-MOFs-1–7) were synthesized by adjusting the ratio of Co^{2+} and Cu^{2+}. The specific morphology of the different Co/Cu-MOFs can be clearly observed through the SEM images, as shown in Fig. 2a and S2.† It can be observed that the particle size of Co/Cu-MOFs-1–7 is about 300–500 nm. Additionally, the structure of Co/Cu-MOFs-3 is further discussed. The composition of Co/Cu-MOFs-3 can be proved by the

EDX elemental mapping data and EDX spectrum, as shown in Fig. 2(b–f). The C, Co, and Cu elements were uniformly distributed in Co/Cu-MOFs-3, which confirms the co-doping of cobalt and copper in Co/Cu-MOFs.

3.2 Catalytic degradation of DOX

3.2.1 Effect of Co/Cu-MOFs. The effect of Co/Cu-MOFs with different metal ratios on DOX degradation was investigated, as shown in Fig. 3. It is clear that DOX removal by different Co/Cu-MOFs varied, but all the removal rates were above 65%. In particular, the removal rate by Co/Cu-MOFs-7 was 100%, and the removal rate by Co/Cu-MOFs-3 was 82.45%. During the first 30 minutes for adsorption–desorption equilibrium, Co/Cu-MOFs-5–7 showed better adsorption than that of Co/Cu-MOFs-1–4, which can be explained by the increase in the proportion of Cu^{2+} increasing the number of pores of Co/Cu-MOFs to facilitate the adsorption of DOX.

It is interesting that the removal rates by Co/Cu-MOFs-5–6 dropped sharply after adding PMS. This can be explained by the concentration of residual DOX in the solution being greatly reduced because a large amount of DOX was adsorbed by Co/Cu-MOFs. After the quencher methanol was added, the determination of DOX concentration absorbance was affected, and the actual removal rate was 89%. The concentration of doxorubicin in the solution can be determined from the working curve of doxorubicin.
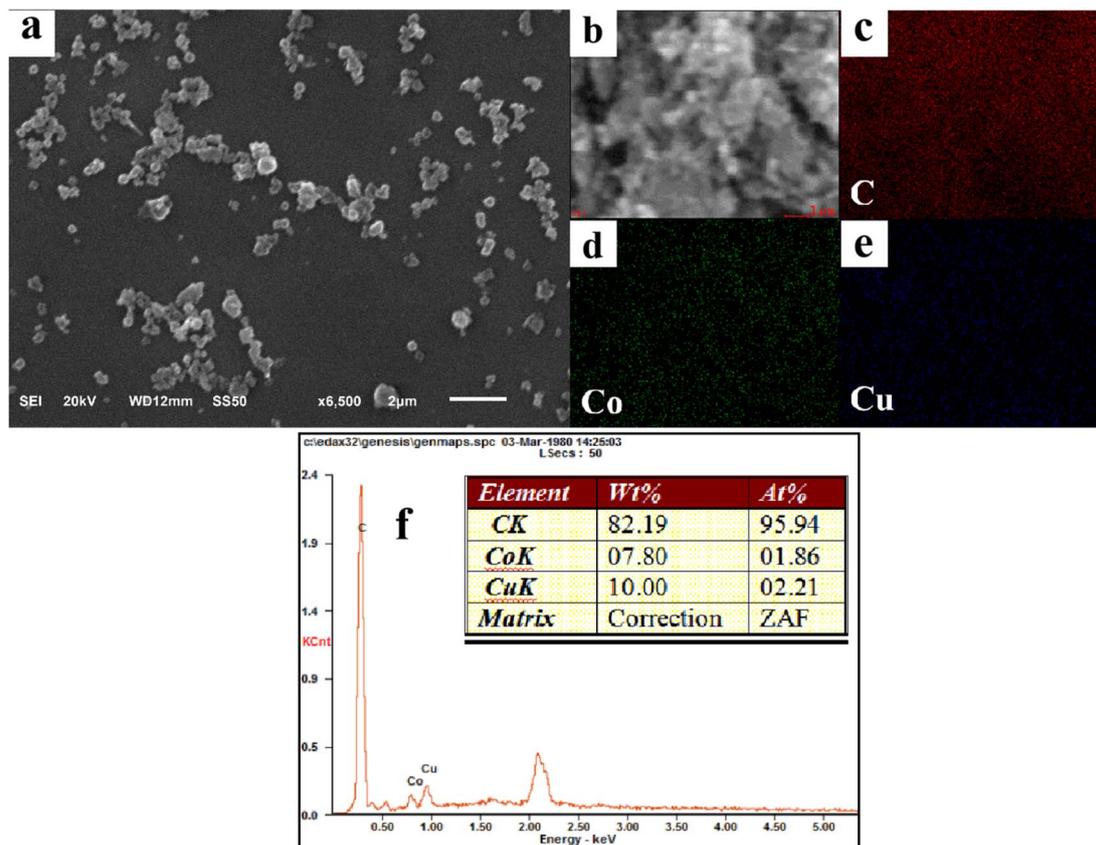
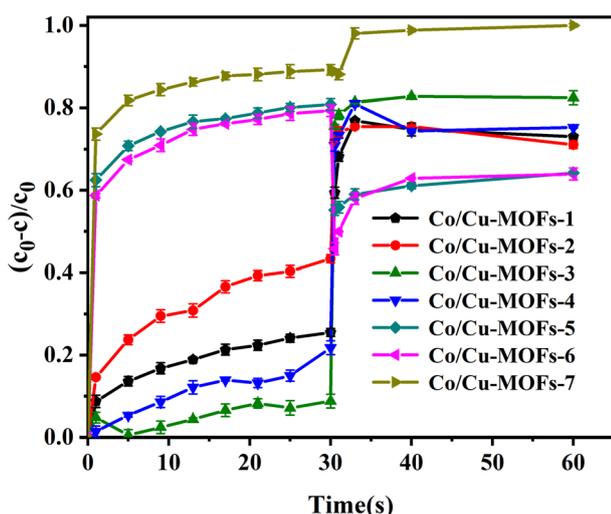Fig. 2   (a) SEM image of Co/Cu-MOFs-3, (b−e) elemental mapping and (f) EDX spectrum of Co/Cu-MOFs-3.

Fig. 3   The effect of different Co/Cu-MOFs on DOX removal.

Co^{2+} is believed to be one of the best metal ions for the catalytic activation of PMS[41] therefore, increasing the Co in Co/Cu-MOFs is more conducive to the progress of the degradation process. It can be seen that after PMS was added, the degradation rate of Co/Cu-MOFs-1–4 increased rapidly. However, the ratio of Co in Co/Cu-MOFs-1–2 is larger than that of Co/Cu-

MOFs-3, indicating that the ratio of Co^{2+} and Cu^{2+} is important to the degradation. Since Co/Cu-MOFs-3 had the lowest adsorption and the best degradation, Co/Cu-MOFs-3 was selected for further experiment.

The pore size distribution was measured by a nitrogen adsorption and desorption experiment, and the result is shown in Fig. S4.† The specific surface area of Co/Cu-MOFs-3 was determined to be 130.470 m^2 g^{-1}. Based on the pore size distribution curves of Co/Cu-MOFs-3, an obvious mesoporous distribution can be observed in the ranges 3–5 nm and 6–9 nm, indicating that the Co/Cu-MOFs have a mesoporous structure. Generally, mesoporous materials show better performance than microporous materials due to less resistance to the penetration of guest molecules in adsorption and/or catalytic degradation. In order to further explore the degradation process, the degradation experiment of Co/Cu-MOFs-3 (simplified to Co/Cu-MOFs) was investigated in detail.

3.2.2 Effect of oxidants. The effect of oxidants was studied, as shown in Fig. 4. The catalytic degradation process was basically completed within 150 s. When H_2O_2 and peroxodisulfate (PDS) were used as oxidants, the degradation rates for DOX were 13% and 21%, respectively. The results showed that the catalytic degradation was not satisfactory when H_2O_2 or PDS were used as an oxidant to be activated by Co/Cu-MOFs. In comparison, when PMS was used as an oxidant, the degradation rate reached 65% in only 10 s and 80% after 150 s, indicating rapid and
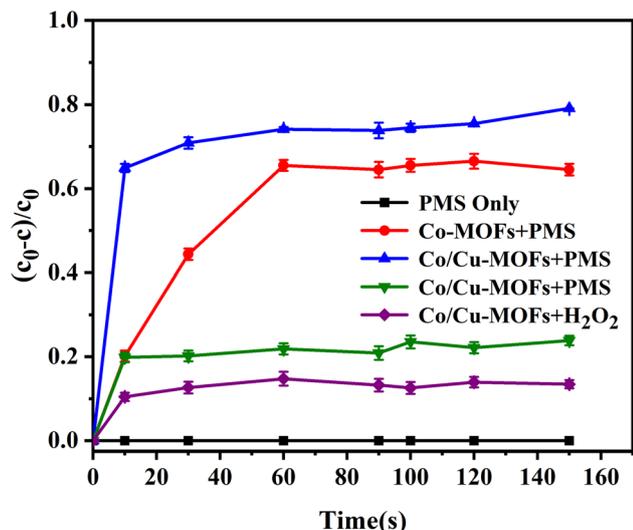
Fig. 4 The influence of the synthesis of different oxidants on the degradation of DOX.

efficient DOX degradation in the Co/Cu-MOFs-PMS system. The reason for the unsatisfactory effect of catalyst Co/Cu-MOFs activation of H_2O_2 to generate ˙OH to degrade doxorubicin may be that H_2O_2 can only react with metal ions over a narrow pH range. In this experiment, the pH was about 4.5 to 5.5, which is not conducive to the activation of H_2O_2. In addition, The O–O bonds of the –O_3S–O–O–SO_3-structures in PDS are symmetric, causing PDS to be more difficult to activate, compared to PMS.[11] Another reason is probably that the molecular size of PMS matches the porous structure of Co/Cu-MOFs more closely than that of PDS or H_2O_2. Co/Cu-MOFs can adsorb PMS, thereby increasing the contact area between PMS and DOX, leading to the rapid degradation of DOX. All in all, when PMS is used as an oxidant, better DOX catalytic degradation can be obtained.

The DOX degradation by Co-MOFs and Co/Cu-MOFs were compared when PMS was selected as oxidant. It was clear that the DOX degradation by Co/Cu-MOFs was better than that by Co-MOFs. Due to the synergistic effect of the two active metals,

cobalt and copper, the interfacial electron transfer will be accelerated, thus generating more SO_4^{-}˙ to promote the catalytic degradation process. This can be further confirmed by the EIS Nyquist plots in Fig. S5.† Co/Cu-MOFs exhibited a smaller semicircle than Co-MOFs within a high-frequency region in the EIS Nyquist plots, which illustrates that the introduction of copper definitely accelerates the electron transfer rate on the catalyst surface.[42] This indicates that the synergistic effect between bimetals can achieve better catalytic activity.

3.2.3 Effect of the amount of PMS and Co/Cu-MOFs. In order to explore the degradation effect on doxorubicin under different conditions, a control experiment was designed (pH = 5.5, T = 25 °C, C_0 = 0.01 g L^{-1}). Fig. 5a demonstrates that the degradation rate reached 80% in just 10 seconds when the amount of Co/Cu-MOFs added was 50 mg, exhibiting the high efficiency of Co/Cu-MOFs activation for PMS. It can be clearly seen that with the increase in Co/Cu-MOFs, the degradation rate of DOX was accelerated. The reason for this phenomenon may be that the enlargement of the catalyst provides more abundant reactive sites, resulting in the generation of more reactive radicals.[43] Furthermore, the effects of PMS concentration are shown in Fig. 5b. In addition, the result of the degradation rate of DOX increasing from 59.7% to 73.4% within just 10 seconds demonstrates that increasing the PMS concentration from 5 to 50 g significantly enhances the catalytic performance. Several studies have shown that a higher PMS dosage may also lead to decreased removal because of the competition from SO_4^{-}˙ with excess PMS.[44] However, this phenomenon was not observed in the PMS dosage range that we investigated, indicating that active radical production in the system of Co/Cu-MOFs/PMS overcomes the competitive effect of PMS. In a word, the bimetallic MOFs catalyst has a considerable degradation effect on doxorubicin hydrochloride.

3.3 Degradation mechanism

In order to gain insight into the degradation mechanism, the effects of ˙OH and SO_4^{-}˙ in the catalytic degradation process were investigated by adding different quenchers, and the
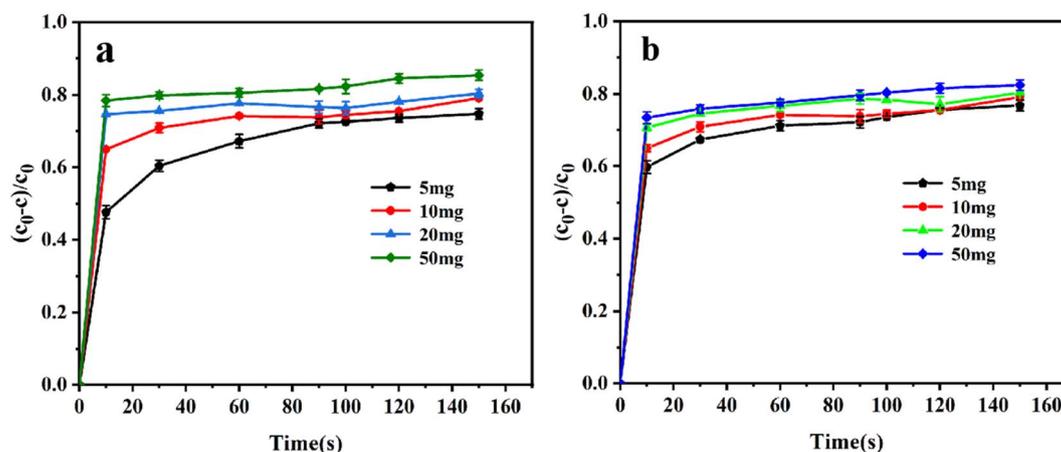

Fig. 5 The effect of the amount of Co/Cu-MOFs (a) and PMS (b) on degradation.

experimental results are shown in Fig. 6a. *tert*-Butanol (TBA) is used to capture ˙OH, methanol is used to capture $SO_4^-˙$, and ethanol can capture both ˙OH and $SO_4^-˙$. After TBA was added, the degradation efficiency was similar to that before adding the quencher, which indicated that ˙OH did not play a major role in the degradation process. After methanol and ethanol were added, the degradation efficiency was greatly reduced, indicating that $SO_4^-˙$ played a decisive role in the degradation process.

To investigate the activation method of PMS by the prepared catalyst, XPS spectra of the catalyst before and after reaction were recorded. As shown in Fig. 6b, an XPS full-range scan of Co/Cu-MOFs indicates the successful co-doping of copper and cobalt into the catalyst. For the Co 2p spectrum in the fresh catalyst (Fig. 6c), two peaks located at 780.2 and 796.5 eV represent Co $2p_{3/2}$ and Co $2p_{1/2}$, which implies that only Co(II) exists in the catalyst. Meanwhile, two satellite peaks located at 785.9 eV and 802.8 eV were also recorded, indicating that the cobalt in Co/Cu-MOFs is present in a high-spin Co^{2+} state.[45,46] Fitting the peak of Co $2p_{3/2}$ in the catalyst after the oxidation process (Fig. 6d), two peaks appear at 779.9 and 781.1 eV, indicating the presence of Co(II) and Co(III), respectively, on the surface of Co/Cu-MOFs.[47] After DOX degradation, the Co(II) in Co/Cu-MOFs is consumed to activate the autolysis of PMS and converted to Co(III) (eqn (1)). The Co(III) are re-converted to Co(II) by capturing electrons (eqn (2)), which inhibits the production of reactive oxygen species (ROS) and causes a decrease in catalyst activity. As shown in Fig. 6e, the Cu 2p spectrum of the fresh catalyst can be fitted into three components, corresponding to

Cu(I) (932.4 eV and 952.2 eV), Cu(II) (934.0 eV and 954.1 eV) and weak satellite peaks (941.1 and 943.5 eV).[48] Furthermore, the high-resolution XPS spectrum of Cu 2p showed a significant change in the Cu(II)/Cu(I) ratio. The $2p_{3/2}$ peak (Fig. 6f) was fitted into two peaks at 932.6 eV and 934.8 eV, corresponding to Cu(I) and Cu(II), respectively. The ratio of Cu(II)/Cu(I) in freshly prepared Co/Cu-MOFs was 0.86 which increased to 1.44 after the oxidation reaction. This suggests the Cu^+ activation of PMS self-decomposition and production of $SO_4^-˙$, as shown in eqn (3) and (4). Meanwhile, Co(III) is reduced by Cu(I) to Co(II), which is capable of activating PMS(eqn (5)). Then, $SO_5^-˙$ can react with OH^- to produce ˙OH, while $SO_4^-˙$ can be converted to ˙OH *via* oxidation of water (eqn (6) and (7)).[49] Finally, $SO_4^-˙$ and ˙OH attack DOX to achieve efficient degradation (eqn (8)).

In the above transformation process, it can clearly be seen that the doping of copper ions can not only activate HSO_5^- by itself, but can also promote the generation of Co^{2+}, thereby generating more $SO_4^-˙$ to improve the degradation performance. Combined with the above analysis, the mechanisms of the PMS activation and ROS evolution processes are proposed in Fig. 7.
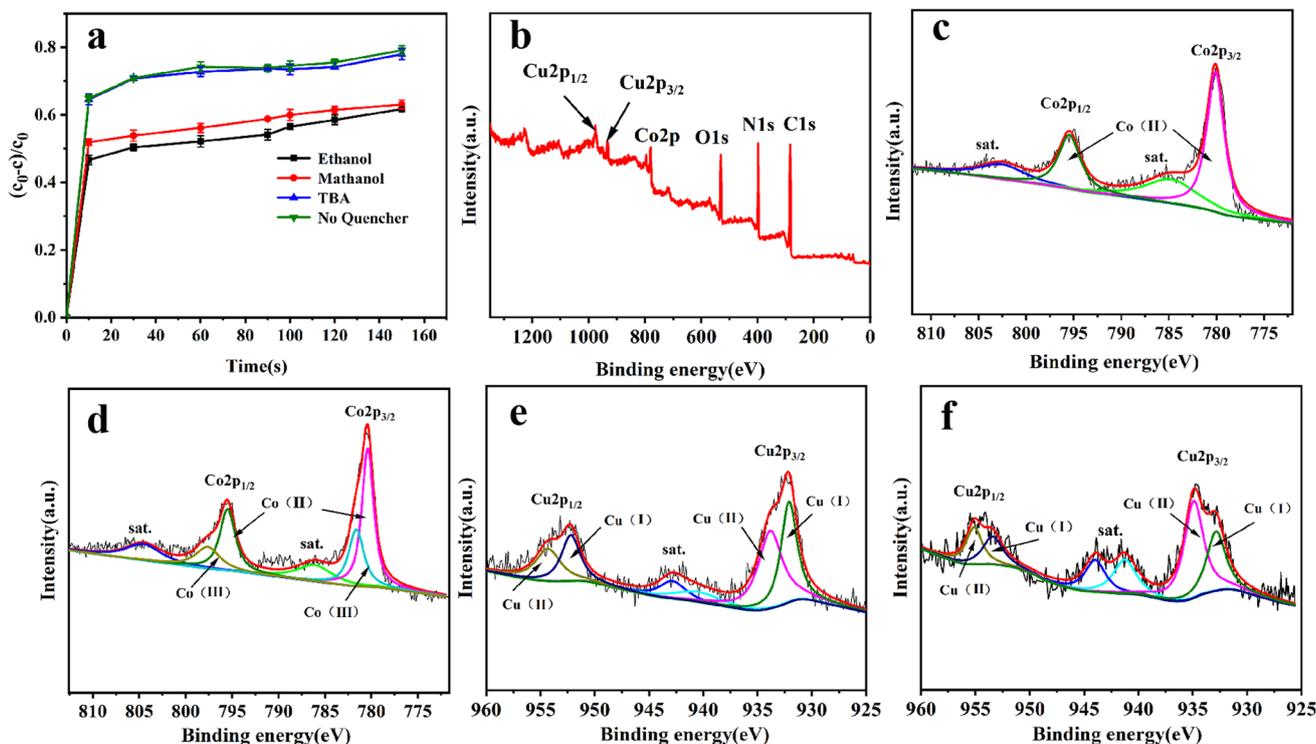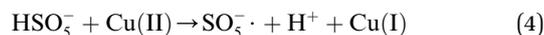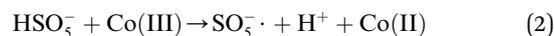
$$HSO_5^- + Co(II) \rightarrow SO_4^-˙ + Co(III) + OH^- \quad (1)$$

$$HSO_5^- + Co(III) \rightarrow SO_5^-˙ + H^+ + Co(II) \quad (2)$$

$$HSO_5^- + Cu(I) \rightarrow SO_4^-˙ + Cu(II) + OH^- \quad (3)$$

$$HSO_5^- + Cu(II) \rightarrow SO_5^-˙ + H^+ + Cu(I) \quad (4)$$

Fig. 6 (a) The effect of different quenchers on DOX degradation; (b) XPS full-range scan of Co/Cu-MOFs; Co 2p spectra of Co/Cu-MOFs before (c) and after (d) the DOX degradation reaction; Cu 2p spectra of Co/Cu-MOFs before (e) and after (f) the DOX degradation reaction.
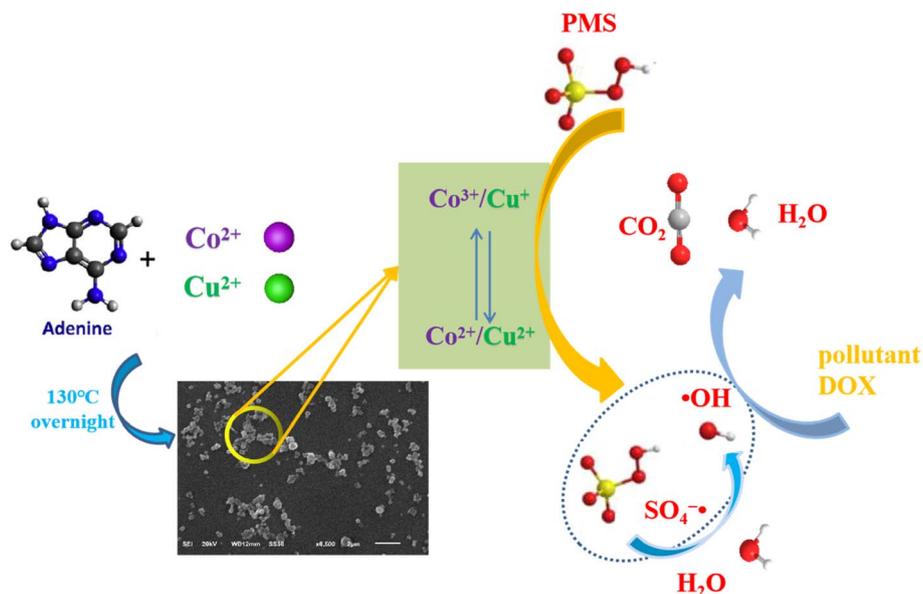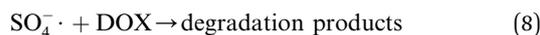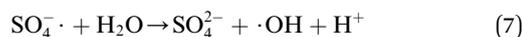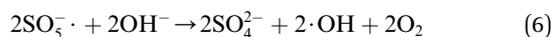
Fig. 7 Schematic illustration of the reaction mechanisms in the Co/Cu-MOFs/PMS system.

$$Co(III) + Cu(I) \rightarrow Co(II) + Cu(II) \tag{5}$$

$$2SO_5^- \cdot + 2OH^- \rightarrow 2SO_4^{2-} + 2 \cdot OH + 2O_2 \tag{6}$$

$$SO_4^- \cdot + H_2O \rightarrow SO_4^{2-} + \cdot OH + H^+ \tag{7}$$

$$SO_4^- \cdot + DOX \rightarrow \text{degradation products} \tag{8}$$
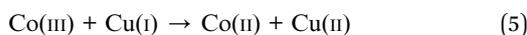
ESI-MS was used to analyze the remaining solution before the reaction, during the degradation process, and after the treatment by the MOFs catalyst and PMS, and the resulting spectra are shown in Fig. S7(a)–(c).† During the degradation process and after the reaction, no DOX was detected, and the presence of large-mass species ($m/z > 300$) was detected. This indicated that the Co/Cu-MOFs-PMS system has a satisfactory degradation effect on DOX, and the structure of DOX was destroyed to change it into molecules with smaller mass. On the

other hand, because the degradation process is very complicated, unstable species produced through recombination and cyclization can be detected, but it is difficult to accurately identify them. A possible structure of the massive species ($m/z > 300$) produced during the reaction is shown in Fig. S7(d).†

3.4 Recycling experiment and stability

The usefulness of a catalyst depends on its reusability. To assess the reusability and stability of Co/Cu-MOFs in PMS activation, four consecutive experiments of DOX degradation were conducted under the same reaction conditions (Fig. 8a). Except for normal washing and drying, the Co/Cu-MOFs had not undergone any subsequent treatment. After 3 cycles, the degradation rate could still reach more than 55% within 10 s and 68% after 150 s. The degradation rate did not change significantly, which showed the sustainability of Co/Cu-MOFs as a catalyst in the degradation of DOX. The ion concentration of the metal
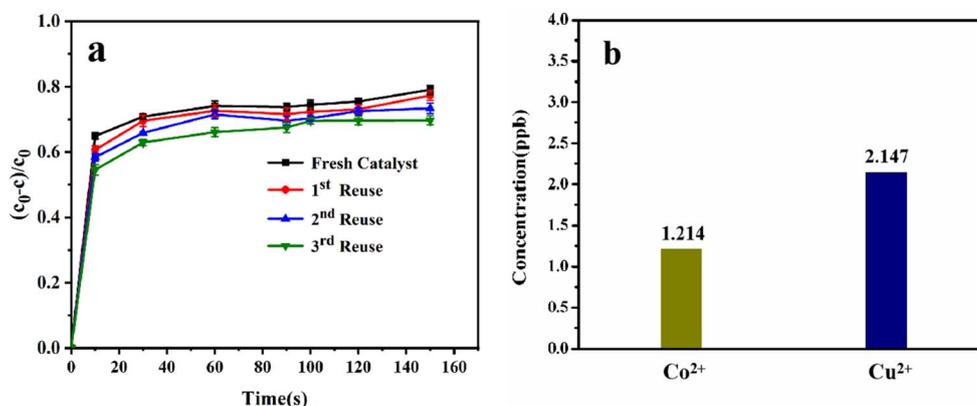

Fig. 8 (a) Recyclability of Co/Cu-MOFs for DOX removal; (b) ion leaching rate.

leaching solution was measured by ICP-MS. As shown in Fig. 8b, the concentration of free Co^{2+} in the solution was 1.214 ppb, and the concentration of free Cu^{2+} in the solution was 2.147 ppb. The concentrations of the two metal ions in the solution were extremely low, so the impact on the degradation process and secondary pollution of the environment are negligible. The water stability of Co/Cu-MOFs can be demonstrated by dynamic light scattering (DLS) measurement. The DLS measurement result is shown in Fig. S5.† The average particle size of the Co/Cu-MOFs is about 550 nm, and it is about 500 nm after 24 h. There is no significant change, indicating the stability of Co/Cu-MOFs-3 in water. The FT-IR and XRD spectra of Co/Cu-MOFs-3 after three cycles of use are shown in Fig. S6.† It can be seen that there is no obvious change, further proving the stability and practicality of Co/Cu-MOFs.

4. Conclusion

A series of Co/Cu-MOFs with different Co/Cu ratios were synthesized via a facile solvothermal process and exhibited excellent PMS activation performance to eliminate DOX from aqueous solution. It was found that successful doping with copper ions can hopefully accelerate the electron transfer of the catalyst, thus generating more $SO_4^{-\cdot}$ to promote the catalytic degradation process. As a result, Co/Cu-MOFs can remove more than 80% of low-concentration DOX in only 10 s. Besides, Co/Cu-MOFs was proved to have good stability during the catalytic degradation process and could still reach more than 55% within 10 s after 3 cycles. Overall, a highly efficient catalytic agent Co/Cu-MOFs for DOX degradation was obtained for the first time, and it could be an attractive option to reduce the potential ecological harm of DOX in environmental water.

Conflicts of interest

There are no conflicts to declare.

Acknowledgements

References

1 Z. L. Wu, Y. P. Wang, Z. K. Xiong, Z. M. Ao, S. Y. Pu, G. Yao and B. Lai, Core-shell magnetic Fe₃O₄@Zn/Co-ZIFs to activate peroxymonosulfate for highly efficient degradation of carbamazepine, Appl. Catal., B, 2020, 277, 119136–119150.

2 J. K. Nam, A. R. Kim, S. H. Choi, J. H. Kim and Y. J. Lee, An antibody against l1 cell adhesion molecule inhibits cardiotoxicity by regulating persistent DNA damage, Nat. Commun., 2021, 12, 3279–3296.

3 H. Ju, S. Li, Y. J. Xu, G. Zhang and J. Zhang, Intensive livestock production causing antibiotic pollution in the yinma river of northeast china, Water, 2019, 11, 2006–2021.

4 X. G. Hu, Q. X. Zhou and Y. Luo, Occurrence and source analysis of typical veterinary antibiotics in manure, soil, vegetables and groundwater from organic vegetable bases, northern China, Environ. Pollut., 2010, 158, 2992–2998.

5 L. L. Gao, Q. He, J. F. Xing and Z. Q. Ge, Removal of doxorubicin by magnetic copper phosphate nanoflowers for individual urine source separation, Chemosphere, 2020, 238, 124690–124699.

6 M. Barczaka, R. Dobrowolski, P. Borowski and D. A. Giannakoudakis, Pyridine-, thiol- and amine-functionalized mesoporous silicas for adsorptive removal of pharmaceuticals, Microporous Mesoporous Mater., 2020, 299, 110132–110139.

7 L. F. Cusioli, H. B. Quesada, M. B. de Andrade, R. G. Gomes and R. Bergamasco, Application of a novel low-cost adsorbent functioned with iron oxide nanoparticles for the removal of triclosan present in contaminated water, Microporou Mesoporous Mater., 2021, 325, 11328–11336.

8 M. Liu, Q. Liu, Z. Zang and R. Han, Adsorptive removal of sulfosalicylic acid from aqueous medium by iron(iii)-loaded magnetic chitosan/graphene oxide, J. Colloid Interface Sci., 2022, 606, 1249–1260.

9 Y. Wang, L. Wang, Y. Zhang, X. Mao, W. Tan, Y. Zhang, X. Wang, M. Chang, R. Guo and B. Xia, Perdisulfate-assisted advanced oxidation of 2,4-dichlorophenol by bio-inspired iron encapsulated biochar catalyst, J. Colloid Interface Sci., 2021, 592, 358–370.

10 J. Li, Y. Liu, X. Ren, W. Dong, H. Chen, T. Cai, W. Zeng, W. Li and L. Tang, Soybean residue based biochar prepared by ball milling assisted alkali activation to activate peroxydisulfate for the degradation of tetracycline, J. Colloid Interface Sci., 2021, 599, 631–641.

11 H. Q. Sun, C. Kwan, A. Suvorova, H. M. Ang, M. O. Tadé and S. B. Wang, Catalytic oxidation of organic pollutants on pristine and surface nitrogen-modified carbon nanotubes with sulfate radicals, Appl. Catal., B, 2014, 154–155, 134–141.

12 X. Chen, W. Wang, H. Xiao, C. Hong and Z. Xue, Accelerated TiO₂ photocatalytic degradation of Acid Orange 7 under visible light mediated by peroxymonosulfate, Chem. Eng. J., 2012, 193–194, 290–295.

13 C. Cai, H. Zhang, X. Zhong and L. Hou, Ultrasound enhanced heterogeneous activation of peroxymonosulfate by a bimetallic Fe–Co/SBA-15 catalyst for the degradation of Orange II in water, J. Hazard. Mater., 2015, 283, 70–79.

14 W. J. Ren, J. K. Gao, C. Lei, Y. B. Xie, Y. R. Cai, Q. Q. Ni and J. M. Yao, Recyclable metal-organic framework/cellulose aerogels for activating peroxymonosulfate to degrade organic pollutants, Chem. Eng. J., 2018, 349, 766–774.

15 Z. M. Liu, Z. M. Gao and Q. Wu, Activation of persulfate by magnetic zirconium-doped manganese ferrite for efficient degradation of tetracycline, Chem. Eng. J., 2021, 423, 130283–130294.

16 X. Zhang, M. Feng, R. Qu, H. Liu, L. Wang and Z. Wang, Catalytic degradation of diethyl phthalate in aqueous

solution by persulfate activated with nano-scaled magnetic $CuFe_2O_4$/MWCNTs, *Chem. Eng. J.*, 2016, **301**, 1–11.

17 Y. Deng and R. Zhao, Advanced oxidation processes (AOPs) in wastewater treatment, *Curr. Pollut. Rep.*, 2015, **1**, 167–176.

18 L. F. Garcia, E. K. G. Moreno, L. B. Brito, G. A. R. D. Oliveira, J. J. Linares and E. D. S. Gil, Effective degradation of the antineoplastic doxorubicin by electrochemical oxidation on boron doped diamond, *J. Electroanal. Chem.*, 2020, **870**, 114252–114258.

19 R. Zhang, P. Sun, T. H. Boyer, Z. Lin and C. H. Huang, Degradation of pharmaceuticals and metabolite in synthetic human urine by UV, UV/H_2O_2, and UV/PDS, *Environ. Sci. Technol.*, 2015, **49**, 3056–3066.

20 C. Luo, M. Feng, V. K. Sharma and C. H. Huang, Oxidation of pharmaceuticals by ferrate(VI) in hydrolyzed urine: effects of major inorganic constituents, *Environ. Sci. Technol.*, 2019, **53**, 5272–5281.

21 O. Abida, M. Kolar, J. Jirkovsky and G. Mailhot, Degradation of 4-chlorophenol in aqueous solution photoinduced by Fe(III)-citrate complex, *Photochem. Photobiol. Sci.*, 2012, **11**, 794–802.

22 X. Deng, L. L. Yang, H. L. Huang, Y. Y. Yang, S. Q. Feng, M. Zeng, Q. Li and D. S. Xu, Shape-defined hollow structural Co-MOF-74 and metal nanoparticles@Co-MOF-74 composite through a transformation strategy for enhanced photocatalysis performance, *Small*, 2019, **15**, 1902287–1902293.

23 C. Wang, J. Kim, J. Tang, M. Kim, H. Lim, V. Malgras, J. You, Q. Xu, J. Li and Y. Yamauchi, New strategies for novel mof-derived carbon materials based on nanoarchitectures – sciencedirect, *Chem*, 2020, **6**, 19–40.

24 K. Zhang, D. D. Sun, C. Ma, G. L. Wang, X. L. Dong and X. X. Zhang, Activation of peroxymonosulfate by $CoFe_2O_4$ loaded on metal-organic framework for the degradation of organic dye, *Chemosphere*, 2020, **241**, 125021–1125033.

25 L. Y. Wang, H. Xu, J. K. Gao, J. M. Yao and Q. C. Zhang, Recent progress in metal-organic frameworks-based hydrogels and aerogels and their applications, *Coord. Chem. Rev.*, 2019, **398**, 213016–213042.

26 J. Cao, Z. H. Yang, W. P. Xiong, Y. Y. Zhou, Y. R. Peng, X. Li, C. Y. Zhou, R. Xu and Y. R. Zhang, One-step synthesis of Co-doped UiO-66 nanoparticle with enhanced removal efficiency of tetracycline: simultaneous adsorption and photocatalysis, *Chem. Eng. J.*, 2018, **353**, 126–137.

27 B. Lei, M. Wang, Z. Jiang, W. Qi, R. Su and Z. He, Constructing redox-responsive metal-organic framework nanocarriers for anticancer drug delivery, *ACS Appl. Mater. Interfaces*, 2018, **10**, 16698–16706.

28 C. Racles, M. F. Zaltariov, M. Silion, A. M. Macsim and V. Cozan, Photo-oxidative degradation of doxorubicin with siloxane MOFs by exposure to daylight, *Environ. Sci. Pollut. Res.*, 2019, **26**, 19684–19696.

29 S. Zhang, H. He, F. Sun, N. Zhao, J. Du, Q. Pan and G. Zhu, A novel adenine-based zinc(II) metal-organic framework featuring the Lewis basic sites for heterogeneous catalysis, *Inorg. Chem. Commun.*, 2017, **79**, 55–59.

30 J. An, O. K. Farha, J. T. Hupp, E. Pohl, J. I. Yeh and N. L. Rosi, Metal-adeninate vertices for the construction of an exceptionally porous metal-organic framework, *Nat. Commun.*, 2012, **3**, 604–609.

31 T. Li, D. L. Chen, J. E. Sullivan, M. T. Kozlowski, J. K. Johnson and N. L. Rosi, Systematic modulation and enhancement of CO_2:N_2 selectivity and water stability in an isoreticular series of bio-MOF-11 analogues, *Chem. Sci.*, 2013, **4**, 1746–1755.

32 Z. Tao, X. Zhang, S. Wang, H. Niu and Y. Cai, Spatial confinement of a Co_3O_4 catalyst in hollow metal-organic frameworks as a nanoreactor for improved degradation of organic pollutants, *Environ. Sci. Technol.*, 2015, **49**, 2350–2357.

33 R. Wu, C. Bi, X. Zhang, J. Wang, L. Wang, C. Fan, M. Wang, F. Shao, N. Li, Z. Zong and Y. Fan, Construction of two cobalt based bi-functional metal-organic frameworks for enhancing electrocatalytic water oxidation and photocatalytic disposals of hazardous aromatic dyes, *Mol. Catal.*, 2021, **505**, 111450–111459.

34 J. An, S. J. Gei and N. L. Rosi, High and selective CO_2 uptake in a cobalt adeninate metal-organic framework exhibiting pyrimidine- and amino-decorated pores, *J. Am. Chem. Soc.*, 2010, **132**, 38–39.

35 J. Xu, J. Gao, Y. Liu, Q. Li and L. Wang, Fabrication of In_2O_3/Co_3O_4-palygorskite composites by the pyrolysis of In/Co-MOFs for efficient degradation of methylene blue and tetracycline, *Mater. Res. Bull.*, 2017, **91**, 1–8.

36 Z. Li, X. Tang, G. Huang, X. Luo and K. Liu, Bismuth MOFs based hierarchical Co_3O_4-Bi_2O_3 composite: an efficient heterogeneous peroxymonosulfate activator for azo dyes degradation, *Sep. Purif. Technol.*, 2020, **242**, 116825–116835.

37 J. Thomas-Gipson, G. Beobide, O. Castillo, M. Fröba, A. Luque, S. Pérez-Yáñez and P. Román, Paddle-wheel shaped copper(II)-adenine discrete entities as supramolecular building blocks to afford porous supramolecular metal-organic frameworks (SMOFs), *Cryst. Growth Des.*, 2014, **14**, 4019–4029.

38 M. R. Azhar, P. Vijay, M. O. Tadé, H. Sun and S. Wang, Submicron sized water-stable metal organic framework (bio-MOF-11) for catalytic degradation of pharmaceuticals and personal care products, *Chemosphere*, 2017, **196**, 105–114.

39 J. An, S. J. Geib and N. L. Rosi, High and selective CO_2 uptake in a cobalt adeninate metal-organic framework exhibiting pyrimidine- and amino-decorated pores, *J. Am. Chem. Soc.*, 2010, **132**, 38–39.

40 X. Y. Ma, Z. H. Liu, Y. L. Yang, L. D. Zhu, J. Deng, S. J. Lu, X. Y. Li and A. M. Dietrich, Aqueous degradation of artificial sweeteners saccharin and neotame by metal organic framework material, *Sci. Total Environ.*, 2021, **761**, 143181–143192.

41 X. G. Duan, C. Su, J. Miao, Y. J. Zhong, Z. P. Shao, S. B. Wang and H. Q. Sun, Insights into perovskite-catalyzed peroxymonosulfate activation: maneuverable cobalt sites for promoted evolution of sulfate radicals, *Appl. Catal., B*, 2018, **220**, 626–634.

42 R. Zhou, J. Zhao, N. Shen, T. Ma, Y. Su and H. Ren, Efficient degradation of 2,4-dichlorophenol in aqueous solution by peroxymonosulfate activated with magnetic spinel FeCo$_2$O$_4$ nanoparticles, *Chemosphere*, 2018, **197**, 670–679.

43 Z. Y. Xiao, Y. Li, L. Fan, Y. X. Wang and L. Li, Degradation of organic dyes by peroxymonosulfate activated with water-stable iron-based metal organic frameworks, *J. Colloid Interface Sci.*, 2021, **589**, 298–307.

44 F. Liu, J. Cao, Z. H. Yang, W. P. Xiong, Z. Y. Xu, P. P. Song, M. Y. Jia, S. W. Sun, Y. R. Zhang and X. X. Zhong, Heterogeneous activation of peroxymonosulfate by cobalt-doped mil-53(al) for efficient tetracycline degradation in water: coexistence of radical and non-radical reactions, *J. Colloid Interface Sci.*, 2021, **581**, 195–204.

45 R. Ma, J. Liang, K. Takada and T. Sasaki, Topochemical synthesis of Co-Fe layered double hydroxides at varied Fe/Co ratios: unique intercalation of triiodide and its profound effect, *J. Am. Chem. Soc.*, 2011, **133**, 613–620.

46 Q. Yang, H. Choi, S. R. Al-Abed and D. D. Dionysiou, Iron–cobalt mixed oxide nanocatalysts: heterogeneous peroxymonosulfate activation, cobalt leaching, and ferromagnetic properties for environmental applications, *Appl. Catal., B*, 2009, **88**, 462–469.

47 A. T. Gu, P. Wang, K. W. Chen, E. D. Miensah, C. H. Gong, Y. Jiao, P. Mao, K. Chen, J. L. Jiang, Y. Liu and Y. Yang, Core-shell bimetallic Fe-Co MOFs to activated peroxymonosulfate for efficient degradation of 2-chlorophenol, *Sep. Purif. Technol.*, 2022, **298**, 121461–121474.

48 P. H. Ling, Q. Zhang, T. T. Cao and F. Cao, Versatile three-dimensional porous Cu@Cu$_2$O aerogel networks as electrocatalysts and mimicking peroxidases, *Angew. Chem., Int. Ed.*, 2018, **130**, 6935–6940.

49 L. M. Dong, Y. M. Li, X. P. Chen, D. Zhang and Y. H. Guan, Zif-67 loaded on Fe$_3$O$_4$-MnO$_2$ as efficient peroxymonosulfate activator for rapid degradation of carbamazepine, *Adv. Mater. Interfaces*, 2021, 2100178–2100188.